Toward deep-space object detection in persistent wide field of view camera arrays

Garrett Fitzgerald
United States Space Force

Zachary Funke
Air Force Research Lab

Alexander Cabello
Algoritics

Vijayan Asari
University of Dayton

Justin Fletcher
United States Space Force

ABSTRACT

Persistent, static telescope arrays leverage a scalable imaging architecture to enable detection of dim deep-space objects while maintaining a wide field of view. The PANDORA (Persistent AND Optically Redundant Array) system, a 5×9 array of commercial-off-the-shelf cameras, is an exemplar of this maturing sensing concept located at the Air Force Maui Optical and Supercomputing site. The PANDORA system is designed to capture $20^\circ\times120^\circ$ wide field of view (WFOV) images of the night sky at a rate of two frames per minute, requiring advanced processing strategies to rapidly detect and track objects of interest. Wide area motion imagery (WAMI) object detection methods that extract scene object features are found to be effective in this WFOV space object detection and tracking application, and are used to demonstrate the exploitation capabilities of the PANDORA sensor system. In this work, we apply WAMI-inspired methods to the passive WFOV space object detection problem, with performance measured using a synthetic PANDORA dataset. We report the performance of three WAMI-inspired techniques for geosynchronous equatorial orbit (GEO) object detection, providing baseline GEO object detection measurements in PANDORA imagery.

DISTRIBUTION A. Approved for public release: distribution is unlimited.
Public Affairs release approval #AFRL-2021-3020

1. INTRODUCTION

Ground-based electro-optical (EO) telescopes are routinely used to discover, track, and characterize resident space objects (RSOs), and are foundational to the establishment and maintenance of space situational awareness (SSA). As the population of near-Earth RSOs grows, the demand for ground-based EO observations grows in proportion. This presents a dilemma: how should one allocate finite EO observations so as to ensure awareness of this larger and more diverse population of RSOs, given that dimmer and more distant objects are detectable only by scarce, large EO telescopes? Narrow field-of-view (NFOV) telescopes provide a means by which to detect these dimmer objects, but must be cued and can observe only a comparatively small fraction of the sky. By contrast, wide field of view (WFOV) optical systems can detect RSOs over larger regions of the sky, but are blind to dimmer objects. One solution to this dilemma is to divide labor between wide and narrow field of view telescopes [1]. This approach, in turn, motivates the creation and utilization of WFOV EO systems. Optical systems using commercial off the shelf (COTS) camera arrays can acquire imagery of the sky, passively collecting low resolution data on the concurrent activity of hundreds of satellites with reasonable sensitivity. This data can then be used to track a large fraction of the RSO population, freeing up collection capacity for articulating EO systems, while also providing tasking information.

The PANDORA 5×9 array, developed by Tau Technologies, utilizes 9 neighboring fields of stacked imagery to acquire a 20°×120° field of view of the sky oriented along the GEO belt. Completed stacked imagery is processed at a rate of 1/30 Hz with an effective exposure time of 60 seconds per frame, accomplished by alternating exposures between common-field cameras. The sensor array uses 5 cameras in common-field to compose co-added individual fields with a SNR improvement of $\sqrt{5}$, with each field capturing a 20°×15° view of sky. With overlap between the 9 fields, the total field of view of the system is 20°×120°, providing the ability to persistently and passively monitor RSOs. The PANDORA system yields 9 (5776×4224×16b) images two times per minute, after registration and stacking of common field images. This corresponds to hundreds of gigabytes of image data each night. PANDORA data volume and velocity (the 9 fields compose over 220 megapixels in total, every 30 seconds), combined with the millions of bright stars in crowded fields, and the low resolution of RSOs (about 3×3 pixels for GEOs), complicate object detection in PANDORA wide FOV imagery. In this work, we introduce techniques to address this challenging object detection problem.

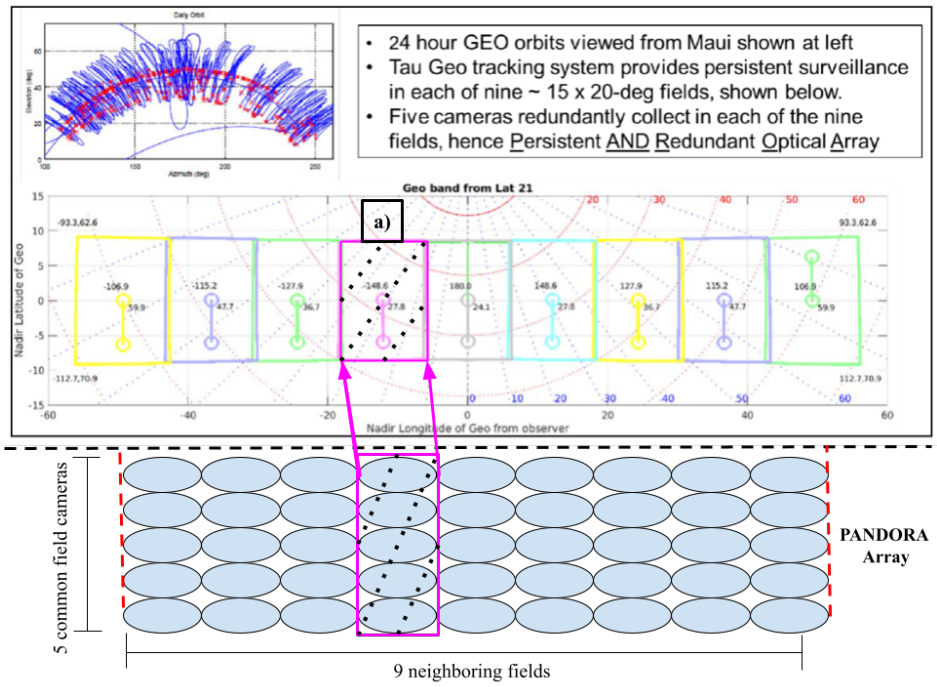

Fig. 1: PANDORA array geometry relative to total 20×120 FOV, with a single 20°×15° field, **a)** highlighted with its corresponding 5 overlapping sensors.

PANDORA provides nightly persistent deep space surveillance at the Air Force Maui Optical and Space Surveillance Site (AMOS), which motivates an image processing pipeline to exploit this data. Due to the limited literature surrounding passive WFOV satellite detection, we explore an architecture in which the GEO detection problem is framed as a WAMI (Wide Area Motion Imagery) object detection problem. WAMI provides a rich literature, including algorithms relevant to WFOV image data with a similar feature space. The architecture proposed in this paper implements three conceptually separate methods of object detection, all of which are based in classical WAMI methodologies adapted to GEO RSO detection in PANDORA imagery. These three approaches are contrasted in performance for object detection on a synthetic dataset, SatSim PANDORA. These baseline methods and results for exploitation of PANDORA data may serve as a benchmark for future studies, culminating with an optimal solution for the utilization of this important sensing concept.

An overview of related works is detailed in Section 2, including a review of similar sensor concepts and applicable WAMI efforts. Section 3 describes the SatSim PANDORA dataset used in this paper. Section 4 details the image processing pipeline developed, including the three object detection algorithms used. Section 5 details experiments executed to quantify object detection performance. Section 6 summarizes results of contributions of this paper along with plans for future work.

2. RELATED WORKS

Focal plane array sensing concepts in the visible regime which achieve all-sky coverage have not been widely studied in the application of detecting and tracking GEO objects. Although orbit estimation models have been formulated for this problem [2], the computer vision problem of exploiting all-sky data with object detection algorithms requires a novel approach, as explored in this paper. We make the distinction that while this sensing concept as a whole is not novel, there do not exist any image processing techniques for autonomously detecting stationary or near-stationary GEO RSOs in WFOV data. Our overall goal is to explore a baseline for image processing performance on such a system, with considerations given to tangential problems in the realm of SSA, astronomy, and wide area surveillance.

The notion of utilizing a collaborative system of shared SSA custody for satellite tracking between a passive, all-sky system and higher resolution telescopes has been explored in recent years, notably with the Raven-class telescope [3], and with a PANDORA system for detection of low earth orbit (LEO) objects [4]. Other COTS camera arrays used for various SSA applications such as [5], and [6], have shown the effectiveness of using co-added sensor exposures of a common field of view to achieve an improved SNR of low light objects. PANDORA implements this COTS co-added sensing concept, with an improved SNR proportional to the number of overlapping sensors [7]. Like PANDORA, the sensor arrays in [5], and [6] are cheap and scalable, utilizing COTS components. Unlike PANDORA, these WFOV systems are applied to such problems as star streak detection and general synoptic surveys, and have not been used for GEO object monitoring.

Similar to PANDORA, some recent optical astronomy initiatives have taken an indiscriminate approach to data collection, including synoptic surveys such as those in progress with the Vera Rubin Telescope, or LSST [8]. These approaches require comprehensive data management strategies [9], and the development of computer vision algorithms to sift through large quantities of data. However, systems collecting optical data in this manner have not yet been used in the detection and tracking of GEO objects, or any relatively stationary space objects similar to GEO satellites. We aim to create methods to process PANDORA image data, allowing for the system to be employed in autonomous monitoring of GEO objects' orbit determinations, catalog maintenance, and anomaly detection.

Without computer vision methods available for any related sensors, the problem of detecting satellites in crowded and large fields requires shifting from the realm of SSA and WFOV astronomy into a well-known class of research, which can be leveraged in the development of PANDORA's image processing strategies. In order to exploit image data from the PANDORA system, we frame the object detection as a Wide Area Motion Imagery (WAMI) problem. WAMI literature is rich in algorithm development for object detection in WFOV imagery, and has demonstrated success in a wide range of applications. WAMI architecture performance on similar problems provides context for the PANDORA processing pipeline [10, 11, 12].

WAMI object detection algorithms generally rely on something that is not applicable to PANDORA data: a static background. The standard process for WAMI detection pipelines involve frame differencing and background subtraction, resulting with candidate regions of object motion in which feature detection techniques are employed [13]. As PANDORA image background is not static, this approach is not acceptable for our use case. If GEO objects were

completely stationary temporally, a reverse to this process could yield regions of the frame with no motion. However, this temporal scene feature is not applicable, as GEO objects are not completely stationary. WAMI algorithms of interest are those which can detect objects based on their local features [14], [15]. Detection algorithms in these papers are used as inspiration for the detection algorithms explored in this paper. With a breadth of WAMI object schemes as inspiration for the PANDORA processing pipeline, we adapt WAMI methodologies for satellite detection in WFOV imagery of PANDORA.

The approaches considered in this paper are all classical in nature, and do not employ deep learning methodologies; this may seem regressive when considering the state of the art in object detection, but the classical approach is deliberate. Computer vision object detection approaches utilizing neural networks have been proven to broadly outperform the best classical object detection algorithms, notably with work demonstrated in Faster R-CNN [16], ResNet [17], and YOLO 9000 [18]. However, the detection problem in these papers use datasets with object candidates comprising most of the image frame [19], while in PANDORA imagery, a given GEO object may be 3×3 pixels in a 220MP image. This large search space, combined with the relative size of objects compared to the scene size, render the direct adoption of proven CNNs for object detection unsuitable. With the goal of this paper being to provide a baseline of results for PANDORA imagery, we start the process of exploiting data with classical algorithms, which have been proven in WAMI literature to be effective in object detection and tracking. However, it is vital to be aware of WAMI object detection schemes which employ deep learning.

Of note, some recent efforts in WAMI have extended the use of spatio-temporal neural networks to achieve state of the art in WAMI moving object detection [20, 21, 22, 23]. With an outpouring of success in these papers, it would seem that a similar solution would be desired for the PANDORA system. While the extension of deep learning has shown success in WAMI object detection in these works, they are nonetheless narrow in application, and not immediately valid for the space object detection problem. The necessitating characteristics of scene motion, as used in with WAMI data such as WPAFB 2009 and CLIF are not applicable to deep-space imagery. Furthermore, the deep learning methods for object detection in these papers use scene-to-scene object motion to establish bounding boxes of interest within small regions of the full scene. Spatial detectors, like [16-18], can detect objects in small subsections of the scene, but as only subsections of scene data are evaluated, the detection strategies in these papers have not been scaled. While effective in narrow applications, no solutions using spatio-temporal CNNs have been extended to full sets of WAMI data on the order of nightly PANDORA imagery. Nonetheless, while this paper uses classical techniques for WAMI object detection, future works should consider a similar approach to the aforementioned papers [20-23], adapted to deep space object detection. For the time being, we assert that in order to initially exploit PANDORA imagery and provide baseline results for the full extent of the sensor's capability, classical WAMI methods are the most appropriate.

The results of this paper provide a baseline GEO object detection performance for the PANDORA sensor system, requiring the use of synthetic data. Due to the characteristics of PANDORA imagery, namely the sparsity and size of GEO objects in each image, building an annotated dataset via human labelling is a time-intensive and therefore expensive process. As such, there exists no such dataset which would allow for performance of detection algorithms to be quantified on physical data. We instead generate a dataset using the SatSim program, a matured synthetic data generation program which will allow for generation of PANDORA-representative imagery [24]. The SatSim PANDORA dataset generated for this paper is described in detail in the following section.

3. DATASETS

SatSim is a modular high fidelity space scene simulator. SatSim is implemented in TensorFlow, is GPU accelerated, and has a modular interface enabling the rapid generation of large volumes of annotated imagery data. SatSim has been initially employed in [24]. For this study, SatSim was used to produce two datasets, the Catalog Dataset and the Monte Carlo Dataset. Each dataset consists of 1,080 PANDORA simulated images. The Catalog Dataset was generated by propagating an active satellite catalog which included LEO, MEO, and GEO orbit classes. The Monte Carlo Dataset contains 300 randomly injected targets with focal plane transverse velocities typical for GEO satellites.

It should be noted that a single processed PANDORA image consists of 30 individual raw images collected from 5 separate cameras over 60 seconds. The raw images are processed, aligned and combined effectively into a single 60-second image. For this study, we chose to simulate the effective 60-second image as if taken from a single camera exposed over 60 seconds. This method was preferred because it takes significantly less computing resources to generate a single image, whereas simulating each image individually would not have been feasible given limited time

and computing resources. Furthermore, we hypothesized this method would give us a higher likelihood of generating comparable images due to limited access to the PANDORA image processing algorithms and raw PANDORA data.

Using a hyperparameter optimization study, SatSim parameters were calculated to produce images acceptably similar to the real combined PANDORA images. We leveraged the optimizer, HyperOpt [25], to test key SatSim parameters and compare the resulting simulated image from each trial to a real combined PANDORA image. The initial loss function implemented was based on subtracting the simulated image from the real image. Due to imperfections in star alignment between the real and simulated, this loss function favored images that were significantly blurrier than the real image. To account for the star alignment issue, a loss function based on comparing histograms at multiple dynamic ranges was developed, which resulted in SatSim images that were more similar to the real combined PANDORA image.

For the initial optimization study, we searched for the best parameters for the zeropoint, background, and the ensquared energy for a Gaussian point spread function (PSF). A follow up optimization was completed after finding the optimal Gaussian PSF was not able to model the real combined PANDORA images very accurately. For the final optimization, we used SatSim's integration of Physical Optics Propagation in PYthon (POPPY) to generate a higher fidelity PSF [26]. Figure 2 shows a comparison of a simulated star using the optimized PSFs with the real PANDORA data. Table 1 shows the SatSim sensor parameters used in this study.

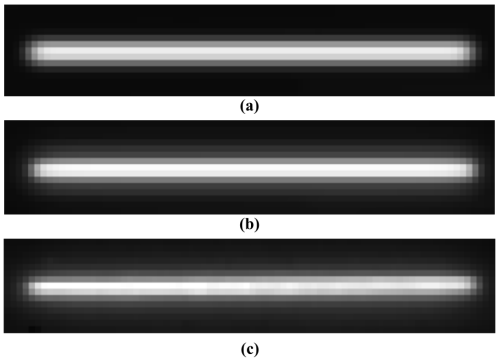

Fig. 2: Comparison of SatSim Simulated Stars and a Real PANDORA Imaged Star Over 60 Seconds. (a) shows a star rendered with SatSim optimized Gaussian PSF; (b) shows a star rendered with SatSim optimized POPPY PSF; (c) shows a real PANDORA imaged star.

Parameter	Value
Width	4224 pixels
Height	5776 pixels
Horz FOV	14.08°
Vertical FOV	19.25°
Background	19.98 mv
Zeropoint	17.72 mv
Gaussian PSF Ensquared energy	0.073
POPPY PSF	Aperture: 0.05m
Exposure	60 seconds

Table 1: SatSim sensor parameters used for this study based on actual camera specifications, astrometry processing of real data, and the SatSim hyperparameter optimization study.

The Catalog Dataset contains satellites propagated from an active satellite catalog. The satellites and the section of the sky were tracked for 120 images over 1 hour. The section of the sky was resampled 9 times providing 1,080 images over 9 hours and 9 different sets of GEO satellites. The satellite brightnesses were randomly sampled between 15.0 visual magnitude (mv) to 9.0 mv for GEO satellites.

The Monte Carlo Dataset contains 300 randomly injected targets per image. The targets and the section of the sky were tracked for 120 images over 1 hour. The targets and section of the sky were resampled 9 times for a total of 2,700 targets and 1,080 images over 9 hours. The targets were randomly injected into the image with a transverse pixel velocity between 0 to 0.125 pixels per second (7.5 pixels per frame) typical of GEO satellites. The brightness of the targets were randomly sampled between 16.5 mv to 11.0 mv.

Figure 3 shows a full field image from the Monte Carlo dataset with annotations. Figure 4 shows the pixel size of each object plotted against its SNR for the Monte Carlo and Catalog datasets, with a line at SNR $= 1$ used to discriminate which objects are prominent relative to scene background. When considering the object population of both datasets, the SNR and size of objects are the most important factors influencing detection performance. While the Monte Carlo dataset will provide a random distribution of object size and SNR, there are many objects with a SNR < 1 which cannot be detected with a single frame detector. The Catalog dataset's objects all have SNRs > 1, but the object population is dominated by 2-pixels objects. This leads to separate challenges in detection performance.

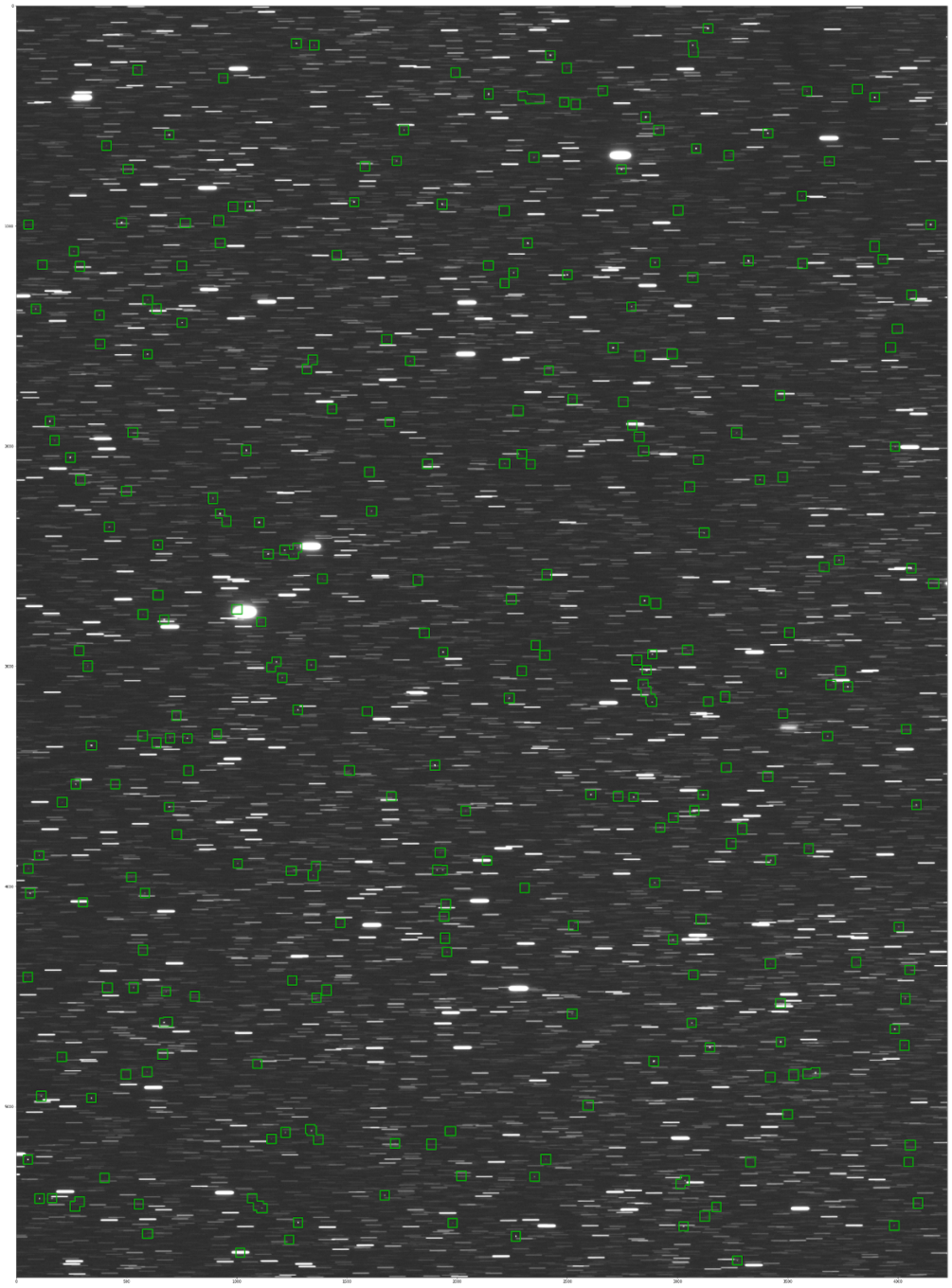

Fig. 3: An Example Image from the Monte Carlo Dataset. Green bounding boxes show where targets have been randomly injected.

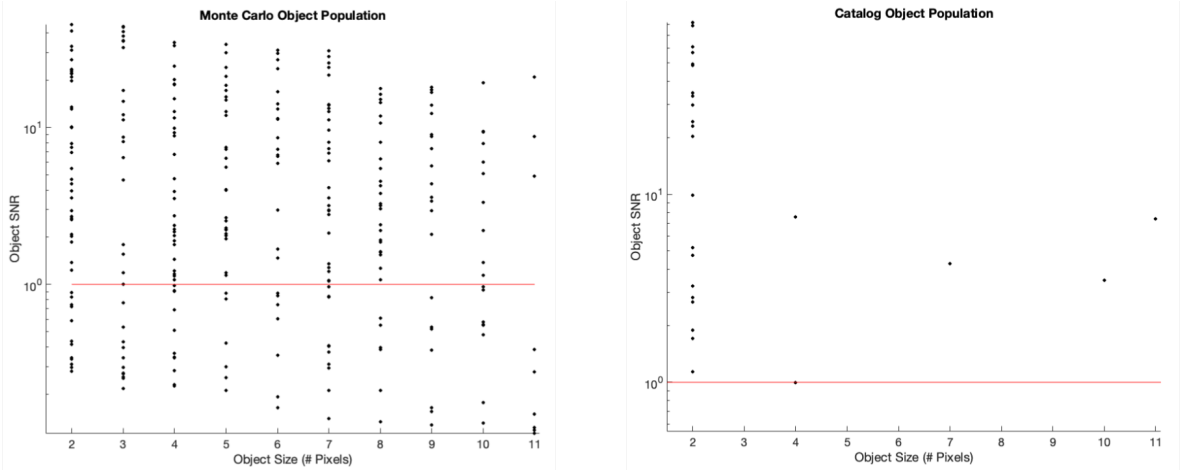

(a) Monte Carlo Dataset (b) Catalog Dataset

Fig. 4: A characterization of SatSim PANDORA GEO object population in a randomly selected single scene, plotting Monte Carlo (a) and Catalog Dataset (b) object brightness and pixel size. A line at SNR = 1 is included, discriminating between prominent objects above background brightness.

4. METHODS

Three algorithms inspired by work in WAMI literature have been implemented for GEO object detection with PANDORA. The first method implements a straightforward feature extractor using SIFT (scale invariant feature transform) with a variable scale space threshold. The second modifies the HOG (histogram of oriented gradients) feature descriptor, calculating overlapping feature vectors to rank areas of the scene with non-horizontal features, which will effectively detect everything that is not a star-streak. The third method of GEO object detection analyzes segmented scene blobs with a calculation of object form factor. These algorithms are feature-based, taking different approaches to provide object detection solutions, and will yield tradeoffs in performance and efficiency. In the case of PANDORA, outside of scene noise, the only objects in frame are stars, GEO objects, and foreground space objects in lower orbit. We can take advantage of the characteristics of each of these objects' typical features to detect GEO objects.

Before applying these detection algorithms, the raw SatSim imagery is processed into segmented and thresholded images. This process first clips the maximum global pixel value at the maximum pixel brightness of an annotated object. While this is not replicable for physical imagery, a similar process can be achieved with the addition of an annotated physical PANDORA dataset. Next, a high boost filter is applied to the image. This nonlinear filtering of the image will sharpen objects relative to the background, and is used to improve relative SNR of detectable objects, as well as rebalance the clipped pixel distributions from the previous step. We then threshold the image using Yen's method [27], which yielded the most detectable objects after thresholding when compared to other methods in [28]. Finally, we apply a morphological filter, using a 3×3 structuring element to augment the continuity of thresholded objects. A diagram visualizing the preprocessing steps used is seen in Figure 5. An example image with a GEO RSO is pictured in Figure 6, showing an image with the HBF applied in a) and the thresholded image in b). With the images thresholded, we then apply detection algorithms to yield candidate centroids of detected objects.

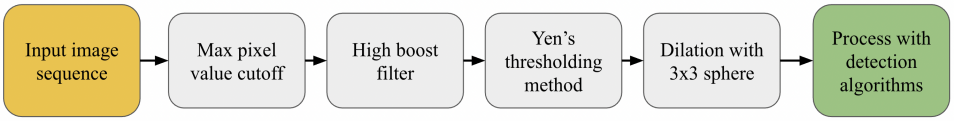

Fig. 5: Preprocessing Flow Chart

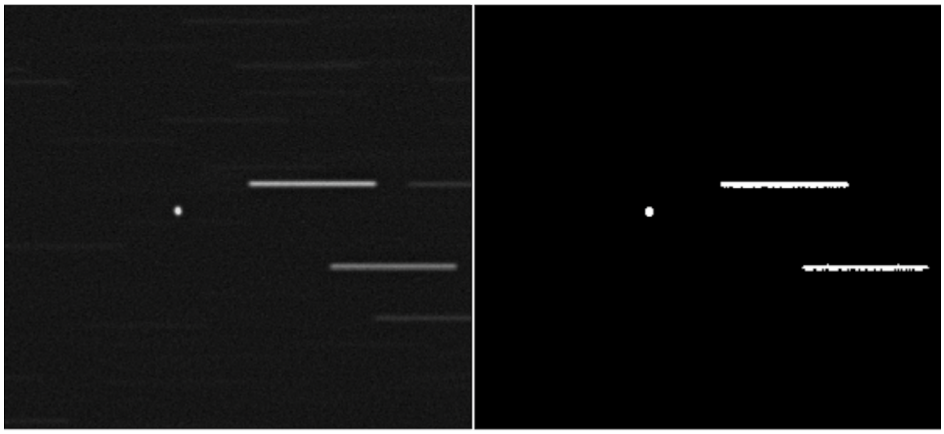

Fig. 6: Image after high boost filtering (left) and after applying Yen's threshold (right).

The first GEO object detection algorithm implemented for this paper uses SIFT (shift invariant feature transformation) feature descriptors. SIFT has been widely adopted in computer vision applications [29]. In WAMI work, it has been used for image registration, as well as object detection [15]. SIFT features are scale invariant, meaning that similar features at different resolutions are comparable via a Difference of Gaussian (DoG) scale space. With this scale invariance comes a measurable notion of feature scale, and to extract GEO objects we alter the peak DoG threshold to extract low-resolution image features. This strategy relies on the similar scale of GEO object size relative to star streaks, and allows for the extraction of image features on the same scale size as GEO objects. Thus, for a single frame, a SIFT detection is defined as all extracted features below a maximum DoG scale space cutoff value. This is an approach which can be directly implemented using the VLFeat computer vision library [30]. The flow diagram of SIFT detection computation steps is seen in Figure 7.

Fig. 7: SIFT Detection Steps

The HOG (histogram of oriented gradients) feature descriptor has been used in numerous image object detection and recognition applications [31], and is a standard method of extracting scene features in WAMI imagery. Often, a cascade of HOG features will be used in conjunction with an SVM or other classifier, creating an object detection scheme with annotated data. We modify HOG to take advantage of star-streak orientation and the relative morphology of GEO objects, and make a point to not rely on a supervised learning algorithm to detect candidate regions, as other HOG detection implementations use. This modification of the HOG algorithm is called HOGOR, or the Histogram of Oriented Gradients, Orientation Rank. First, gradient magnitude and orientation are calculated for cells of pixel size 20×20 for the image. The gradient magnitude is binned into 8 orientation bins, from $-\pi$ to π. The histogram bins of cell orientation are representative of the overall direction of gradient intensity for each 20×20 subsection of the image. The cell's value is 1 if summed orientation bin values for -77.5°:77.5° are greater than the horizontal orientation bins -90° + 90°. This process renders all cells with a part of a horizontal star streak 0, and all other cells 1. This calculation is repeated for 25 to 90 percent overlapping cells, resulting with 9 HOGOR feature vectors per image. The feature vector cells are added together to create a detection heatmap, where regions with heatmap values > 9 are considered object detections. This method, like SIFT, relies on the consistent orientation of star streaks and morphology of GEO objects, however it is much more computationally expensive. A flow diagram for the HOGOR detection scheme is seen in Figure 8.

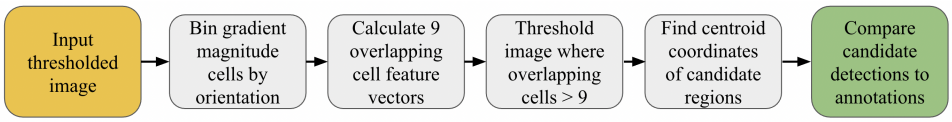

Fig. 8: HOGOR Detection Steps

The third method of GEO object detection uses the thresholded image to perform blob analysis. Image blobs are defined as contiguous connected pixels within a thresholded image. We define the form factor F as

$$F = \frac{(4 * \pi * A)}{p^2}, \tag{1}$$

where A is the blob area and p is the perimeter, in pixels [32]. This calculation will describe how circular a blob is. We elect to use this calculation to discriminate between GEO objects and star streaks, by choosing a variable max F to filter out all star-streak detections, leaving GEO object candidate centroids. The flow chart for calculating detection candidates with the form factor method is seen in Figure 9.

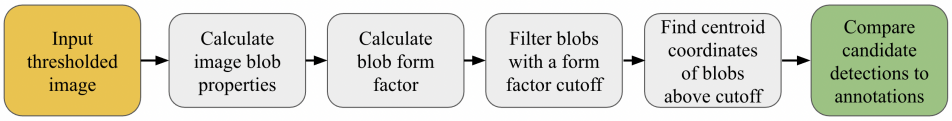

Fig. 9: Form Factor Detection Steps

5. RESULTS

The three object detection algorithms described are applied separately for analysis. In order to generalize performance across the Monte Carlo and the Catalog datasets, we sample frames from different fields at different temporal steps. For both datasets, we randomly select 6 frames out of the total 120 per field, resulting with detections calculated for 54 images for each dataset, as there are 9 fields per dataset. Table 2 shows the parameters used for the detection algorithms.

Detector	Parameter	Parameter Ranges
SIFT	DoG Threshold	{1.2, 1.4, 1.5, 1.6, 1.7, 1.8, 2.0}
HOGOR	% Overlapping Cells	{25, 40, 50, 60, 70, 80, 90}
Form Factor	Form Factor Threshold	{0.3, 0.4, 0.5, 0.6, 0.7, 0.8, 0.9}

Table 2: Detection Algorithm Parameter Ranges

We calculate the precision and recall for these detectors at each value in their parameter range. Precision and recall are performance metrics which are well-known in the field of computer vision detection problems. Precision and recall are calculated with the following equations.

$$Precision = \frac{TP}{TP + FP} \tag{2}$$

$$Recall = \frac{TP}{TP + FN} \tag{3}$$

Here, TP is the number of correct detections, defined as a detector candidate centroid within 5 pixels of an annotated object centroid. FP is the number of false positives in a frame, determined by all detector candidates which are not within the Euclidean distance of 5 pixels of an annotated object centroid. FN is defined as all annotated objects in a

frame which were not detected. With precision and recall measured for each detector's set of parameter ranges, we can find a maximum F_1^* value, where

$$F_1^* = max\left(\frac{2 \times precision \times recall}{precision + recall}\right), \tag{4}$$

can serve as a scalar value to quantify performance of a given detector with a sampled dataset. We calculate the precision and recall for each detector across the 54 sampled images from each dataset for each value in their parameter range, which yields precision and recall curves.

With our image processing approach of first thresholding images before analyzing with a detection algorithm, we consider the performance of the detection algorithms with different subsets of the Monte Carlo and Catalog datasets. First, we find the precision and recall of the detector with all annotations in the dataset, even though many of these low-light GEO RSOs are lost after thresholding. Second, for the Monte Carlo dataset, we consider all objects which are above a SNR of 1. Finally, we will analyze performance on the thresholded imagery considering only annotated objects which had a brightness above the threshold value. Table 3 shows each of the subsets of SatSim PANDORA imagery used to measure performance, with the number of annotated objects being averaged over the 54 samples for each dataset. Note that the Monte Carlo dataset has objects which have a SNR < 1, while the Catalog dataset is generated with all objects' SNR > 1.

Dataset	Number of annotated objects
Monte Carlo All	300
Monte Carlo SNR > 1	210
Monte Carlo Thresholded	72
Catalog All	30
Catalog Thresholded	14

Table 3: Detection Algorithm Parameter Ranges

Table 4 shows the F_1^* scores for each detection method associated with the precision and recall at F_1^*, along with the number of TP, FP, and FN for this F_1^* score. Figure 10 shows the precision/ recall curves for the Monte Carlo (a) and Catalog (b) datasets, showing detection performance for the Monte Carlo SNR > 1, Monte Carlo Thresholded, Catalog All, and Catalog Thresholded. While the detectors determine candidate centroids using the thresholded imagery, we consider their performance with each of the subsets of the datasets in order to generalize the overall system performance of GEO detection in PANDORA imagery.

Dataset	Detector	F_1^*	Precision at F_1^*	Recall at F_1^*	TP at F_1^*	FP at F_1^*	FN at F_1^*
Monte Carlo All	SIFT	0.22	0.246	0.19	62	190	238
Monte Carlo All	HOGOR	**0.366**	0.68	0.25	75	25	225
Monte Carlo All	FF	0.357	0.971	0.219	66	2	234
Monte Carlo SNR > 1	SIFT	0.270	0.28	0.26	55	141	155
Monte Carlo SNR > 1	HOGOR	0.401	0.88	0.26	55	8	210
Monte Carlo SNR > 1	FF	**0.491**	0.96	0.33	69	3	210
Monte Carlo Threshold	SIFT	0.439	0.32	0.7	50	106	22
Monte Carlo Threshold	HOGOR	0.752	0.8	0.71	51	13	21
Monte Carlo Threshold	FF	**0.945**	0.96	0.93	67	3	5
Catalog All	SIFT	0.161	0.11	0.29	9	73	21
Catalog All	HOGOR	**0.634**	0.70	0.58	17	7	13
Catalog All	FF	0.573	0.90	0.421	13	2	6
Catalog Threshold	SIFT	0.313	0.21	0.61	9	34	5
Catalog Threshold	HOGOR	0.659	0.56	0.80	11	9	3
Catalog Threshold	FF	**0.941**	0.940	0.941	13	1	1

Table 4: Single Frame Detection Performance averaged over 54 samples

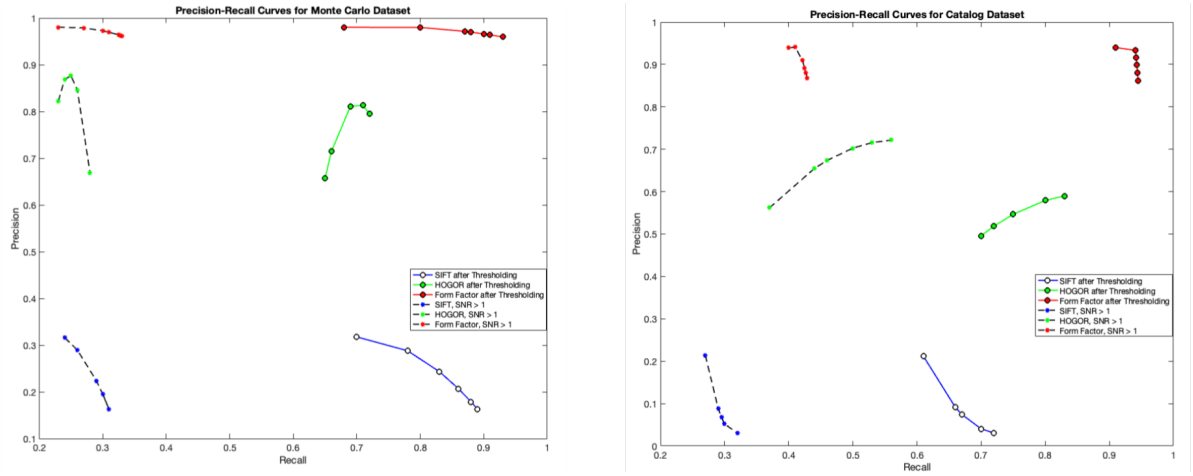

(a) Monte Carlo Dataset

(b) Catalog Dataset

Fig. 10: Precision Recall Curves

First considering results with thresholded objects, we see that the best performing algorithm is with form factor blob analysis. The F_1^* score of 0.94 for both the Monte Carlo and Catalog Thresholded sub-datasets vastly outperforms the SIFT and HOGOR detection algorithms. While this is a very accurate detector, it maintains such a high F_1^* value when only considering thresholded targets. We can draw a distinction that if the image preprocessing pipeline yielded thresholded imagery with a higher percentage of targets, the performance of the detection algorithms would improve in the Monte Carlo All and Catalog All sub-datasets.

Our implementation of SIFT is not an effective detector for this object detection problem, but could be used when we extend the detection analysis to temporal data. SIFT's candidate detection strategy of filtering scene features with a feature DoG scale space threshold yielded both GEO objects and the ends of star-streaks, which have a similar scale space value. If we extended this method to include the feature extraction of temporal scene data, it could be a viable option through filtering objects via scene-to-scene feature motion. However, in the single frame analysis we performed, this method is least effective.

The HOGOR method of extracting scene features, which rank as non-horizontal, works quite well for the single frame GEO detection application. It is precise, but fails to provide detections for obejcts which are not perfectly circular. For example, because we require each of the 9 HOGOR feature vector cells to have a non-horizontal gradient orientation, a single cell which includes a GEO object might only include the top or bottom of the object, yielding a non-positive cell region, and by extension a false negative. This method is expensive, but can be modified to calculate more overlapping features with more bins of gradient orientation, which will improve the single frame HOGOR recall. This method is also scalable via parallism, as each feature vector is caluclated independently. It should be considered for future work, but may require maturation to be deployable on the PANDORA system.

The form factor calulation yields impressive results for the thresholded sub-dataset, and is also the best performing algorithm for each of the other sub-datasets. It is a simple calcluation, and will work as a detector in this feature space as long as we use a 60 second exposure to capture scene data. This long exposure time results with long star-streaks, which will always have a very low form factor. GEO objects, with a low resolution and limited motion, will always have a form factor which is clearly discernable from that of star-streaks. This method is fast to calculate, and will be a very effective autonomous detector for the PANDORA system with improved preprocessing techniques.

Considering the reported detection performance on both datasets, and with the conditions of including detection candidates from thresholded targets and all targets with SNR > 1, there are clear takeaways from this work. First, we can say that morphological analysis of thresholded imagery yields strong results with the form factor calculation. Second, this compelling performance is predicated on the ability to threshold all detectable objects successfully. Because the preprocessing pipeline excludes objects with low SNRs out of thresholded imagery, when considering all annotated objects, the single scene detection algorithms perform poorly. However, we are confident that with further image processing techniques, these methods are viable options for autonomous GEO object detection in PANDORA imagery.

With the overall system goal of detecting and tracking GEO objects, these algorithms serve as the first step exploiting PANDORA imagery for GEO RSO orbit esitmation, anomaly detection, and new-object detection.

6. CONCLUSION AND FUTURE WORK

This work establishes a baseline state of the art approach for GEO object detection in passive WFOV ground based optical sensor systems. The form factor calculation is both the most computationally simple, as well as the best performing detection algorithm from our adoption of WAMI algorithms to this problem. The single frame detection performance which was presented can be generalized to physical PANDORA data based on the accuracy of the SatSim PANDORA dataset. Furthermore, we can quantify performance on physical imagery with the addition of annotated physical PANDORA data. Future work will include the extension of deep learning methodologies to this problem set, including the adoption of spatial-temporal neural networks for object detection. The classical detection methods presented can be improved upon through a more thorough preprocessing pipeline, which will yield more low light targets in the thresholded imagery. These methods can also be extended to the temporal dimension of PANDORA data, which will yield a process of detecting and tracking GEO RSOs.

Acknowledgements
The authors wish to thank the professors of the University of Dayton's Electrical and Computer Engineering department, who helped prepare a litany of classical image processing tools and knowledge, especially from the instruction of Dr. Russell Hardie. We would also like to thank the engineers of Tau Technologies, who matured and delivered the PANDORA system to AMOS.

REFERENCES

[1] Ryan D. Coder and Marcus J. Holzinger. "Multi-objective design of optical systems for space situational awareness". en. In: *Acta Astronautica* 128 (Nov. 2016), pp. 669–684.

[2] Michael D. Schneider and William A. Dawson. "Synthesis of Disparate Optical Imaging Data for Space Domain Awareness". en. In: (Sept. 2016).

[3] Tom Kelecy et al. "Real-time Space Object Capture and Handoff Using Wide Field of View Telescope Development at AMOS". In: *57th International Astronautical Congress*. American Institute of Aeronautics and Astronautics, 2012.

[4] Luis Varela. "Streak Detection in Wide Field of View Images Using Deep Learning and Data Augmentation". en. PhD thesis. New Mexico State University, 2020.

[5] Mariusz Grøtte et al. "All-Sky Image Fusion for a Synoptic Survey Telescope in Arctic and Antarctic Domains". In: (Jan. 2016).

[6] Lucas P. Parker et al. "A heterogeneous telescope array optimized for low surface-brightness imaging". In: *Ground-based and Airborne Instrumentation for Astronomy VIII*. International Society for Optics and Photonics, Dec. 2020.

[7] CY Zhang. "Robust estimation and image combining". In: *Astronomical Data Analysis Software and Systems* 77.IV (1995), p. 514.

[8] Zeljko Ivezic et al. "LSST Survey Strategy". In: 211 (Dec. 2007). Conference Name: American Astronomical Society Meeting Abstracts ADS Bibcode: 2007AAS...21113702I, p. 137.02.

[9] Mario Jurić et al. "The LSST Data Management System". en. In: *arXiv preprint* arXiv:1512.07914 (Dec. 2015).

[10] Erik Blasch et al. "Summary of methods in Wide-Area Motion Imagery (WAMI)". In: *Geospatial InfoFusion and Video Analytics IV; and Motion Imagery for ISR and Situational Awareness II*. Vol. 9089. International Society for Optics and Photonics, June 2014.

[11] Jan Prokaj and Gerard Medioni. "Persistent Tracking for Wide Area Aerial Surveillance". In: 2014, pp. 1186–1193.

[12] Arslan Basharat et al. "Real-time multi-target tracking at 210 megapixels/second in Wide Area Motion Imagery". In: *IEEE Winter Conference on Applications of Computer Vision*. ISSN: 1550-5790. Mar. 2014, pp. 839–846.

[13] Lars Wilko Sommer et al. “A survey on moving object detection for wide area motion imagery”. In: *2016 IEEE Winter Conference on Applications of Computer Vision (WACV)*. Mar. 2016, pp. 1–9.

[14] Theus H. Aspiras, Vijayan K. Asari, and Juan Vasquez. “Gaussian ringlet intensity distribution (GRID) features for rotation-invariant object detection in wide area motion imagery”. In: *2014 IEEE International Conference on Image Processing (ICIP)*. ISSN: 2381-8549. Oct. 2014, pp. 2309–2313.

[15] Alex Mathew and Vijayan K. Asari. “Local region statistical distance measure for tracking in Wide Area Motion Imagery”. In: *2012 IEEE International Conference on Systems, Man, and Cybernetics (SMC)*. ISSN: 1062-922X. Oct. 2012, pp. 248–253.

[16] Shaoqing Ren et al. “Faster R-CNN: Towards Real-Time Object Detection with Region Proposal Networks”. In: *Advances in Neural Information Processing Systems*. Vol. 28. Curran Associates, Inc., 2015.

[17] Kaiming He et al. “Deep Residual Learning for Image Recognition”. In: 2016, pp. 770–778.

[18] Joseph Redmon and Ali Farhadi. “YOLO9000: Better, Faster, Stronger”. In: 2017, pp. 7263–7271.

[19] Tsung-Yi Lin et al. “Microsoft COCO: Common Objects in Context”. In: *Computer Vision – ECCV 2014*. Ed. by David Fleet et al. Lecture Notes in Computer Science. Cham: Springer International Publishing, 2014, pp. 740–755.

[20] Rodney LaLonde, Dong Zhang, and Mubarak Shah. “ClusterNet: Detecting Small Objects in Large Scenes by Exploiting Spatio-Temporal Information”. In: 2018, pp. 4003–4012.

[21] Burak Uzkent, Christopher Yeh, and Stefano Ermon. “Efficient Object Detection in Large Images Using Deep Reinforcement Learning”. In: 2020, pp. 1824–1833.

[22] Yifan Zhou and Simon Maskell. “Detecting and Tracking Small Moving Objects in Wide Area Motion Imagery (WAMI) Using Convolutional Neural Networks (CNNs)”. In: *2019 22th International Conference on Information Fusion (FUSION)*. July 2019, pp. 1–8.

[23] Lars Wilko Sommer, Tobias Schuchert, and Jürgen Beyerer. “Fast Deep Vehicle Detection in Aerial Images”. In: *2017 IEEE Winter Conference on Applications of Computer Vision (WACV)*. Mar. 2017, pp. 311–319.

[24] Justin Fletcher, Ian McQuaid, and Peter Thomas. “Feature-Based Satellite Detection using Convolutional Neural Networks”. In: *Proceedings of the Advanced Maui Optical and Space Surveillance Technologies Conference* (2019), p. 11.

[25] James Bergstra et al. “Hyperopt: a Python library for model selection and hyperparameter optimization”. en. In: *Computational Science & Discovery* 8.1 (July 2015). Publisher: IOP Publishing.

[26] Marshall Perrin et al. “POPPY: Physical Optics Propagation in PYthon”. In: *Astrophysics Source Code Library* (Feb. 2016).

[27] Jui-Cheng Yen, Fu-Juay Chang, and Shyang Chang. “A new criterion for automatic multilevel thresholding”. In: *IEEE Transactions on Image Processing* 4.3 (Mar. 1995). Conference Name: IEEE Transactions on Image Processing, pp. 370–378.

[28] Mehmet Sezgin and Bülent Sankur. “Survey over image thresholding techniques and quantitative performance evaluation”. In: *Journal of Electronic Imaging* 13.1 (Jan. 2004). Publisher: International Society for Optics and Photonics, pp. 146–165.

[29] David G. Lowe. “Distinctive Image Features from Scale-Invariant Keypoints”. en. In: *International Journal of Computer Vision* 60.2 (Nov. 2004), pp. 91–110.

[30] Andrea Vedaldi and Brian Fulkerson. “Vlfeat: an open and portable library of computer vision algorithms”. In: *Proceedings of the 18th ACM international conference on Multimedia*. New York, NY, USA: Association for Computing Machinery, Oct. 2010, pp. 1469–1472.

[31] Qiang Zhu et al. “Fast Human Detection Using a Cascade of Histograms of Oriented Gradients”. In: *2006 IEEE Computer Society Conference on Computer Vision and Pattern Recognition (CVPR’06)*. Vol. 2. ISSN: 1063-6919. June 2006, pp. 1491–1498.

[32] Jaromir Zavadil, Jiri Tuma, and Vitor M. F. Santos. “Traffic signs detection using blob analysis and pattern recognition”. In: *Proceedings of the 13th International Carpathian Control Conference (ICCC)*. May 2012, pp. 776–779.